The 3-hydroxyacyl-CoA dehydratases HACD1 and HACD2 exhibit functional redundancy and are active in a wide range of fatty acid elongation pathways

Received for publication, June 20, 2017, and in revised form, July 19, 2017 Published, Papers in Press, August 7, 2017, DOI 10.1074/jbc.M117.803171

Megumi Sawai[‡1], Yukiko Uchida[‡1], Yusuke Ohno[‡], Masatoshi Miyamoto[‡], Chieko Nishioka[§], Shigeyoshi Itohara[§], Takayuki Sassa[‡], and Akio Kihara[‡2]

From the [‡]Faculty of Pharmaceutical Sciences, Hokkaido University, Sapporo 060-0812 and the [§]RIKEN Brain Science Institute, 2-1 Hirosawa, Wako 351-0198, Japan

Edited by Dennis R. Voelker

Differences among fatty acids (FAs) in chain length and number of double bonds create lipid diversity. FA elongation proceeds via a four-step reaction cycle, in which the 3-hydroxyacyl-CoA dehydratases (HACDs) HACD1–4 catalyze the third step. However, the contribution of each HACD to 3-hydroxyacyl-CoA dehydratase activity in certain tissues or in different FA elongation pathways remains unclear. *HACD1* is specifically expressed in muscles and is a myopathy-causative gene. Here, we generated *Hacd1* KO mice and observed that these mice had reduced body and skeletal muscle weights. In skeletal muscle, *HACD1* mRNA expression was by far the highest among the *HACDs*. However, we observed only an ~40% reduction in HACD activity and no changes in membrane lipid composition in *Hacd1*-KO skeletal muscle, suggesting that some HACD activities are redundant. Moreover, when expressed in yeast, both HACD1 and HACD2 participated in saturated and monounsaturated FA elongation pathways. Disruption of *HACD2* in the haploid human cell line HAP1 significantly reduced FA elongation activities toward both saturated and unsaturated FAs, and *HACD1 HACD2* double disruption resulted in a further reduction. Overexpressed HACD3 exhibited weak activity in saturated and monounsaturated FA elongation pathways, and no activity was detected for HACD4. We therefore conclude that HACD1 and HACD2 exhibit redundant activities in a wide range of FA elongation pathways, including those for saturated to polyunsaturated FAs, with HACD2 being the major 3-hydroxyacyl-CoA dehydratase. Our findings are important for furthering the understanding of the molecular mechanisms in FA elongation and diversity.

Fatty acids (FAs)[3] are major components of lipids. Differences in chain length and the number and position of double bonds generate diversity in FAs and lipids. Most cellular FAs are long-chain FAs (LCFAs; C11–C20), among which C16 and C18 LCFAs are especially abundant. FAs of length ≥C21 are called very-long-chain FAs (VLCFAs). Although the cellular quantities of VLCFAs are much lower than those of LCFAs, VLCFAs possess characteristic functions that cannot be performed by LCFAs. Mutations in yeast and mice resulting in defective VLCFA synthesis are lethal (1–5). Most of the VLCFAs are used as components of sphingolipids but are almost absent in glycerolipids (6, 7). The functions of VLCFAs include stabilization of membrane curvature, membrane microdomain formation, and enhancement of hydrophobicity of lipids at the molecular level, which are important for maintenance of organelle structure and function, cellular signaling, vesicular trafficking, and formation of multilayered lipid structure at the cellular level (8–13). Physiologically, VLCFAs play important roles in skin barrier formation, maintenance of liver integrity, spermatogenesis, neural functions, myelin maintenance and formation, and retinal functions (7, 13–21).

FAs are elongated via the FA elongation cycle in the endoplasmic reticulum, using acyl-CoA as a substrate. In each cycle, the FA chain length is increased by two carbon units. The FA elongation cycle consists of four distinct reactions (condensation, reduction, dehydration, and reduction), and the enzymes involved are conserved among eukaryotes (6, 7, 22) (Fig. 1). In the first reaction (condensation), acyl-CoAs receive two carbon units from malonyl-CoA, generating 3-ketoacyl-CoAs. This step is the rate-limiting step of the FA elongation cycle and is catalyzed by FA elongases (ELOVL1–7 in mammals and Elo1, Fen1/Elo2, and Sur4/Elo3 in yeast) (6, 7, 11, 22–24). The 3-ketoacyl-CoAs are then reduced to (*R*)-3-hydroxy (3-OH) forms by 3-ketoacyl-CoA reductases (KAR/HSD17B12 in mammals and Ifa38/Ybr159w in yeast) (3, 25). Subsequently, 3-OH acyl-CoAs are dehydrated by 3-OH acyl-CoA dehydratases (HACD1/PTPLA, HACD2/PTPLB, HACD3/PTPLAD1, and HACD4/PTPLAD2 in mammals and Phs1 in yeast) (4, 26). Finally, the resulting *trans*-2-enoyl-CoAs are reduced to acyl-CoAs, which now have two more carbons than the original

This work was supported by the Advanced Research and Development Programs for Medical Innovation (AMED-CREST) (to A. K.) of the Japan Agency for Medical Research and Development (AMED), by Grant-in-aid for Scientific Research (A) 26251010 (to A. K.) from the Japan Society for the Promotion of Science, and by Grant-in-aid for Young Scientists (A) 15H05589 (to Y. O.) from Japan Society for the Promotion of Science. The authors declare that they have no conflicts of interest with the contents of this article.

[1] Both authors contributed equally to this work.

[2] To whom correspondence should be addressed: Faculty of Pharmaceutical Sciences, Hokkaido University, Kita 12-jo, Nishi 6-chome, Kita-ku, Sapporo 060-0812, Japan. Tel.: 81-11-706--3754; Fax: 81-11-706-4900; E-mail: kihara@pharm.hokudai.ac.jp.

[3] The abbreviations used are: FA, fatty acid; LCFA, long-chain fatty acid; VLCFA, very-long-chain fatty acid; 3-OH, 3-hydroxy; LC, liquid chromatography; MS/MS, tandem mass spectrometry; *d*, deuterium; 3xFLAG, triple FLAG; FAME, fatty acid methyl ester; DKO, double KO; HMF, His_6, Myc epitope, and triple FLAG; AMPP, *N*-(4-aminomethylphenyl)pyridinium; HACD, 3-hydroxyacyl-CoA dehydratase; F, forward; R, reverse; TECR, *trans*-2-enoyl-CoA reductase; ELOVL, elongation of very-long-chain fatty acid.

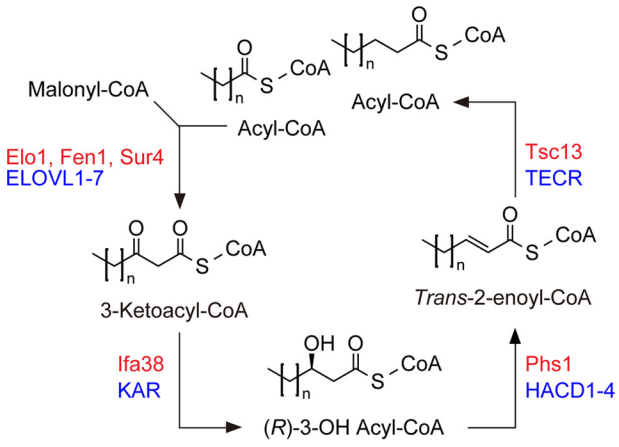

Figure 1. FA elongation cycle. The four reactions in the FA elongation cycle and the enzymes involved (*red,* yeast proteins; *blue*, mammalian proteins) are shown. In one round of the FA elongation cycle, the carbon chain length of acyl-CoA is increased by two, where malonyl-CoA acts as a carbon donor.

acyl-CoAs. This step is catalyzed by *trans*-2-enoyl-CoA reductases (TECR/TER in mammals and Tsc13 in yeast) (2, 25).

The enzymes responsible for the first and third steps of the FA elongation cycle have multiple isozymes in mammals (ELOVL1–7 and HACD1–4). The substrate specificities of the FA elongases ELOVL1–7 have already been determined; each exhibits characteristic substrate specificity toward acyl-CoAs with different chain lengths and numbers of double bonds (6, 7, 11, 22). In contrast, the substrate specificities of HACD1–4 are unknown, mainly due to limitations in the commercial availability of 3-OH acyl-CoA species. We previously demonstrated that purified HACD1–4 all exhibit activity *in vitro* toward the only commercially available 3-OH palmitoyl-CoA substrate (26). In that assay, HACD2 showed the greatest activity and that of HACD4 was the lowest (~16-fold lower than that of HACD2 in terms of V_{max}). *HACD2* mRNA is ubiquitously expressed in tissues (27), and *HACD3* mRNA is expressed in many tissues, such as brain, kidney, liver, and placenta (26). In contrast, expression of *HACD1* and *HACD4* mRNA is restricted to muscle tissue (skeletal muscle and heart) and leukocytes, respectively (26, 28). Mutations in *HACD1* cause myopathy in humans and dogs (29, 30). *Hacd1* KO mice also exhibit a myopathic phenotype, with reduced body weight, muscle mass, muscle force, and muscle fiber diameter (31). During myogenesis, myoblasts are fused into multinucleated myotubes, followed by maturation into myofibers. The fusion process is retarded in *Hacd1* KO myoblasts (31).

In this study, we aimed to identify as-yet-undetermined substrate specificities of HACDs. For this purpose, we performed lipidomics analyses on newly generated *Hacd1* KO mice. Furthermore, the 3-OH acyl-CoA dehydratase activity of each HACD was investigated by FA elongation assay, in which commercially available acyl-CoAs/FAs were used as substrates, instead of direct measurement of 3-OH acyl-CoA dehydratase activity using 3-OH acyl-CoA substrates. Our results indicate that HACD1 and HACD2 exhibit broad substrate specificities. They are active toward saturated, monounsaturated, and polyunsaturated 3-OH acyl-CoAs of long- to very long-chain FAs, with HACD2 exhibiting greater activity than HACD1. In contrast, HACD3 showed only weak activity in saturated and monounsaturated FA elongation pathways, and no HACD4 activity was detected.

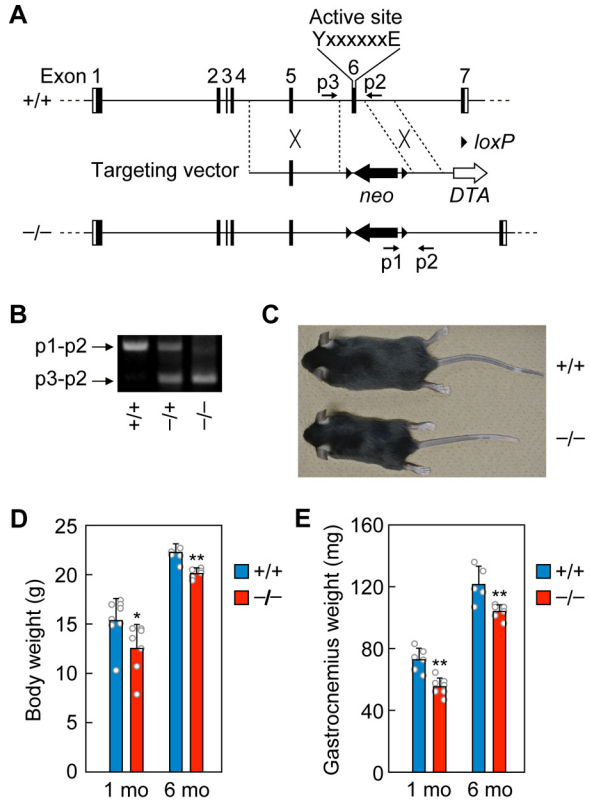

Figure 2. Reduced body and skeletal muscle weights in *Hacd1* KO mice. *A*, schematic representation of the *Hacd1* region in WT (+/+) and *Hacd1* KO (−/−) mice as well as the *Hacd1* gene-targeting vector construct. The positions of the primers (p1, p2, and p3) used for genomic PCR are denoted with *arrows*. *DTA*, diphtheria toxin A gene for negative selection; *neo*, neomycin-resistant gene for positive selection. *B*, genomic DNAs prepared from the tails of $Hacd1^{+/+}$, $Hacd1^{+/-}$, and $Hacd1^{-/-}$ mice were subjected to PCR using primers p1, p2, and p3. The amplified fragments were separated by agarose gel electrophoresis, followed by staining with ethidium bromide. *C*, $Hacd1^{+/+}$ and $Hacd1^{-/-}$ mice at 3 months old. *D* and *E*, body weight (*D*) and gastrocnemius weight (*E*) of female $Hacd1^{+/+}$ and $Hacd1^{-/-}$ mice at 1 and 6 months old. Values represent the means ± S.D. from 5 to 8 mice. Statistically significant differences are indicated (**, $p < 0.01$; *, $p < 0.05$; Student's *t* test). *mo,* month.

Results

Moderate reduction in 3-OH acyl-CoA dehydratase activity in Hacd1 KO mice

To reveal the substrate specificity of HACD1 and the pathogenesis of the myopathy caused by *HACD1* mutations, *Hacd1* KO mice were created. HACD/Phs1 family members contain the active-site residues Tyr and Glu within the fifth transmembrane segment (32, 33). The *Hacd1* KO construct was designed to replace exon 6, which encodes the active-site residues, with a neomycin-resistant gene (Fig. 2*A*). Gene disruption was confirmed by genomic PCR (Fig. 2*B*). The *Hacd1* KO mice exhibited smaller body size (Fig. 2*C*) and reduced body and skeletal muscle (gastrocnemius) weight at 1 and 6 months of age (Fig. 2, *D* and *E*), compared with the control mice, as has been reported previously (31).

In WT skeletal muscle, expression levels of *HACD1* mRNA were much higher than those of other *HACDs* (Fig. 3*A*). How-

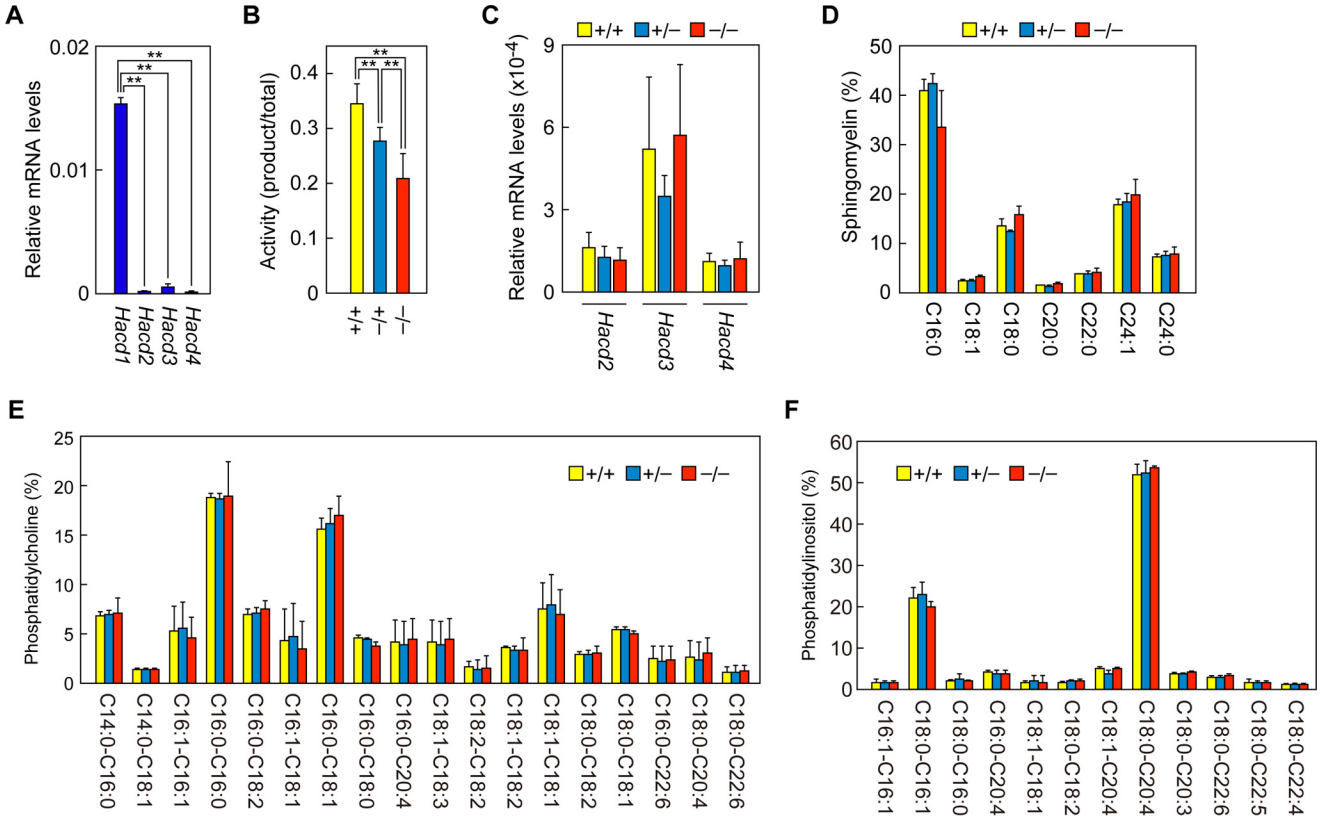

Figure 3. Moderate reduction in 3-OH acyl-CoA dehydratase activity and unchanged membrane lipid composition in *Hacd1* KO mice. *A*, total RNAs prepared from the gastrocnemius of female WT mice at 1 month old were subjected to SYBR Green-based real-time quantitative RT-PCR using specific primers for *Hacd1*, *Hacd2*, *Hacd3*, *Hacd4*, and *Gapdh*. Values represent the means ± S.D. relative to *Gapdh* expression levels from three independent reactions. Statistically significant differences are represented (**, $p < 0.01$; Tukey's test). *B*, total membrane fractions (20 μg of protein) prepared from the gastrocnemius of female *Hacd1*$^{+/+}$, *Hacd1*$^{+/-}$, and *Hacd1*$^{-/-}$ mice at 1 month old were incubated with 0.01 μCi of [^{14}C]3-OH palmitoyl-CoA for 10 min at 37 °C. Lipids were saponified, acidified, extracted, separated by normal-phase TLC, and detected using a BAS-2500 image analyzer. Values represent the means ± S.D. of the ratio of the product lipid radioactivity to total lipid radioactivity from three independent reactions. Statistically significant differences are represented (**, $p < 0.01$; Tukey's test). *C*, total RNAs prepared from the gastrocnemius of female *Hacd1*$^{+/+}$, *Hacd1*$^{+/-}$, and *Hacd1*$^{-/-}$ mice at 1 month old were subjected to SYBR Green-based real-time quantitative RT-PCR using specific primers for *Hacd2*, *Hacd3*, *Hacd4*, and *Gapdh*. Values represent the means ± S.D. relative to *Gapdh* expression levels from seven (*Hacd1*$^{+/+}$ and *Hacd1*$^{-/-}$) or five (*Hacd1*$^{+/-}$) independent experiments. No statistically significant differences were detected between samples using the Tukey-Kramer method. *D–F*, lipids were extracted from the gastrocnemius of *Hacd1*$^{+/+}$, *Hacd1*$^{+/-}$, and *Hacd1*$^{-/-}$ mice at P0, and sphingomyelin (*D*), phosphatidylcholine (*E*), and phosphatidylinositol (*F*) species were analyzed by LC-MS/MS. Values are the means ± S.D. of the quantity of each lipid species containing FAs with the indicated chain length and desaturation number from three independent experiments. No statistically significant differences were detected between the samples by Tukey's test.

ever, the reductions in the 3-OH acyl-CoA dehydratase activity toward 3-OH palmitoyl-CoA in skeletal muscles of *Hacd1* heterozygous KO (*Hacd1*$^{+/-}$) and *Hacd1* homozygous KO (*Hacd1*$^{-/-}$) mice relative to WT mice were relatively small (~20% reduction in *Hacd1*$^{+/-}$ mice and ~40% reduction in *Hacd1*$^{-/-}$ mice; Fig. 3*B*). No compensatory increases in *HACD2*, *HACD3*, or *HACD4* mRNA levels were observed in the *Hacd1* KO skeletal muscle (Fig. 3*C*).

Next, we examined the effect of *Hacd1* gene disruption on the product levels. Because the acyl-CoA products elongated via the FA elongation cycle are mainly used for membrane lipid synthesis, we measured the levels of three major lipid classes in skeletal muscle by liquid chromatography (LC)–tandem mass spectrometry (MS/MS). These were the sphingolipid sphingomyelin (Fig. 3*D*) and the glycerophospholipids phosphatidylcholine (Fig. 3*E*) and phosphatidylinositol (Fig. 3*F*). There were no differences in the levels of these lipids among WT (*Hacd1*$^{+/+}$), *Hacd1* heterozygous KO (*Hacd1*$^{+/-}$), and *Hacd1* homozygous KO (*Hacd1*$^{-/-}$) mice, irrespective of chain lengths (Fig. 3, *D–F*).

To further examine the effect of *Hacd1* gene disruption on the FA elongation cycle, myoblasts were prepared from WT and *Hacd1* KO mice. After differentiation into myotube cells, they were incubated with deuterium (*d*)-labeled FAs for 24 h, and their metabolism was traced by LC-MS/MS analysis. Exogenously added FAs are metabolized to other FAs via elongation and/or desaturation within cells (Fig. 4*A*). When cells were labeled with d_{31}-palmitic acid (C16:0-COOH) (palmitic acid with 31 deuteriums (d_{31})), d_{31}-labeled saturated and monounsaturated C16–C26 FAs were detected in WT cells (Fig. 4*B*). Almost no differences were observed in the compositions of d_{31}-labeled FAs between WT and *Hacd1* KO cells. Furthermore, tracer analyses using d_9-oleic acid (C18:1–COOH) indicated that d_9-oleic acid metabolism was indistinguishable between WT and *Hacd1* KO cells (Fig. 4*C*). Mammals cannot produce *n*-6 and *n*-3 polyunsaturated FAs endogenously, due to a lack of FA Δ12 desaturase and FA Δ15 desaturase, and must therefore obtain these FAs from foods. Food-derived polyunsaturated FAs are subjected to repetitive elongation and desaturation in cells and are converted to other polyunsaturated FAs

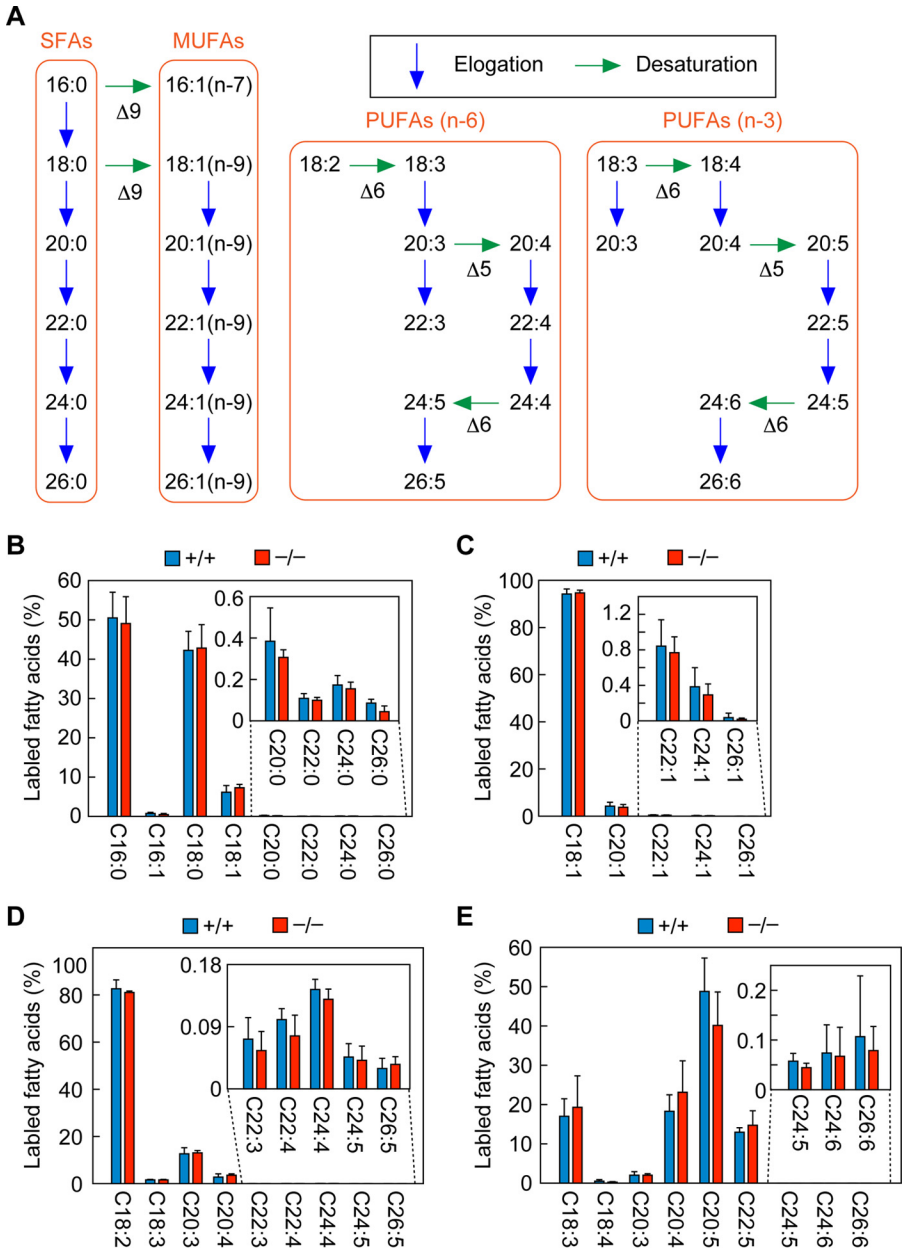

Figure 4. No FA metabolic change in the *Hacd1* KO muscle. *A*, FA metabolic pathways in mammals. FA elongation and desaturation reactions of saturated FAs (SFAs), monounsaturated FAs (MUFAs), and *n*-6 and *n*-3 polyunsaturated FAs (PUFAs) are illustrated. Δ, desaturase. *B–E*, mouse primary cultured myoblasts prepared from WT (+/+) and *Hacd1* KO (−/−) mice at 1 month old were differentiated into myotube cells for 3 days and labeled with 1 μM d_{31}-palmitic acid (*B*), d_9-oleic acid (*C*), d_{11}-linoleic acid (*D*), or d_5-α-linolenic acid (*E*) for 24 h at 37 °C. Lipids were extracted, saponified, derivatized to AMPP amides and analyzed by LC-MS/MS. Values are the means ± S.D. of the quantities of deuterium-labeled FAs with the indicated chain length and desaturation number from three independent experiments. No statistically significant differences were detected between WT and KO samples by Student's *t* test.

(Fig. 4*A*). d_{11}-Linoleic acid (C18:2(*n*-6)-COOH) (Fig. 4*D*) and d_5-α-linolenic acid (C18:3(*n*-3)-COOH) labeling (Fig. 4*E*) experiments revealed that these FAs were metabolized similarly in WT and *Hacd1* KO cells. Thus, disruption of *Hacd1* gene had no apparent effects on membrane lipid composition or the FA elongation cycle.

Redundant substrate specificities of HACD1 and HACD2 in saturated and monounsaturated FA elongation pathways

Relatively weak effects on the 3-OH acyl-CoA dehydratase activity as a result of *Hacd1* gene KO (Fig. 3*B*) suggest redundancy among the HACDs. We previously reported that ectopic expression of *HACD1* or *HACD2* in a *PHS1*-shutoff yeast strain complemented growth defects, whereas neither *HACD3* nor *HACD4* exhibited such activity (26). In WT yeast *Saccharomyces cerevisiae*, the VLCFAs are almost exclusively C26:0 (34), whereas the production of at least some C24:0 VLCFAs is necessary for normal growth (11). Consequently, the results of the growth complementation analysis suggest that both HACD1 and HACD2 possess the ability to produce C24:0 or longer VLCFAs, and therefore that there is some redundancy in their function.

We first examined the activity of HACD1 and HACD2 in the saturated FA elongation pathway, using a yeast system. To minimize the endogenous 3-OH acyl-CoA dehydratase activity, we

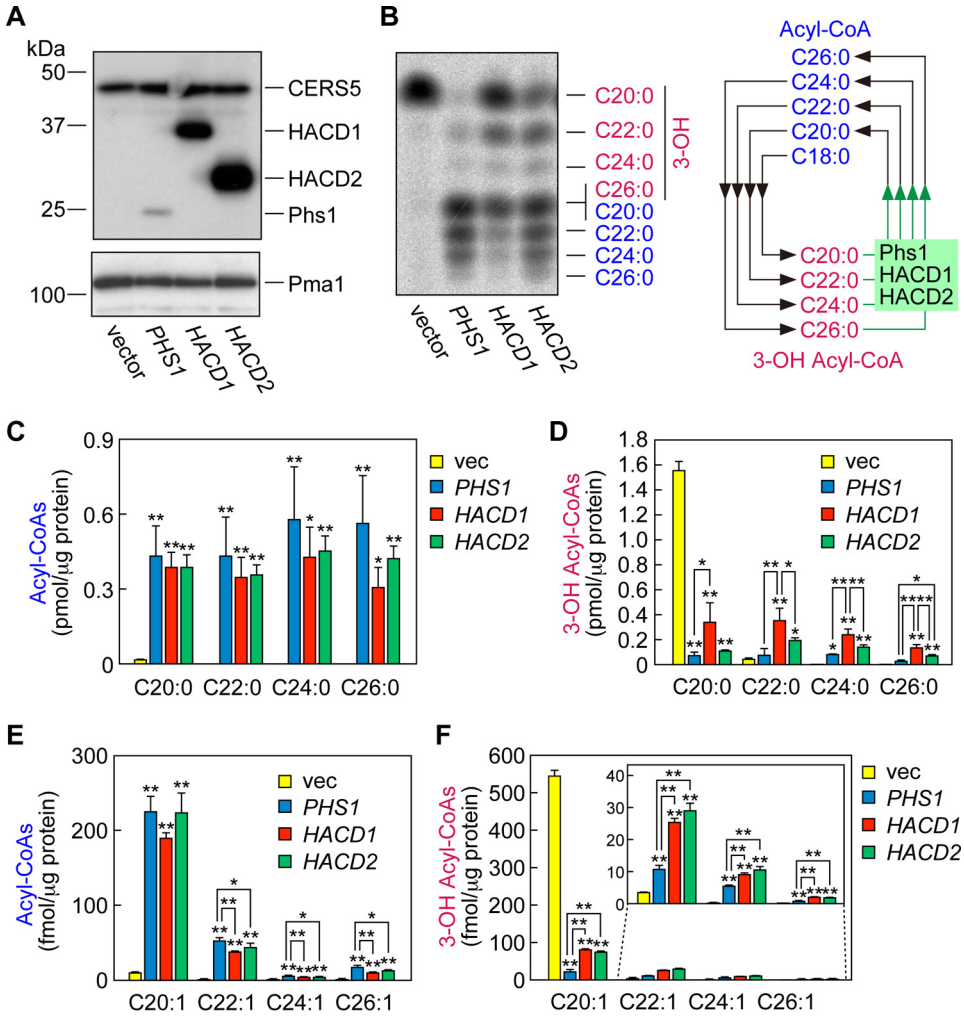

Figure 5. HACD1 and HACD2 exhibit broad substrate specificities toward saturated and monounsaturated 3-OH acyl-CoAs. *A–F*, total membrane fractions were prepared from the yeast KMY81 (*phs1*Δ *htd2*Δ/pAB119 (*3xFLAG-CERS5*)) cells bearing the pAK739 (vector), pRF6 (*PHS1–3xFLAG*), pYS10 (*HMF-HACD1*), or pTN28 (*HMF-HACD2*) plasmid and subjected to immunoblotting with anti-FLAG and anti-Pma1 (membrane protein loading control) antibodies (*A*) and FA elongation assays using [^{14}C]malonyl-CoA (*B*) or [^{13}C]malonyl-CoA (*C–F*). *B*, total membrane fractions (20 μg of protein) were incubated with 75 nCi of [^{14}C]malonyl-CoA and 20 μM stearoyl-CoA for 30 min at 37 °C. After the reaction, lipids were saponified, converted to FAMEs, separated by reverse-phase TLC, and detected using a BAS-2500 image analyzer. The acyl-CoA and 3-OH acyl-CoA intermediates of the FA elongation cycle, starting from stearoyl-CoA (C18:0), are illustrated in the *right panel*. *C–F*, total membrane fractions (20 μg of protein) were incubated with 100 μM [^{13}C]malonyl-CoA and 10 μM stearoyl-CoA (*C* and *D*) or oleoyl-CoA (*E* and *F*) for 30 min at 37 °C. After the reaction, lipids were saponified, derivatized to AMPP amides, and analyzed by LC-MS/MS. Values are the means ± S.D. of the quantities of acyl-CoA derivatives (*C* and *E*) or 3-OH acyl-CoA derivatives (*D* and *F*) with the indicated chain length and desaturation number from three independent experiments. Statistically significant differences are calculated by Tukey's test (**, $p < 0.01$; *, $p < 0.05$). Significant differences are represented by *asterisks* above the lines connecting the bar graphs. Otherwise, the *asterisks* represent significant differences from the vector control. *vec*, vector.

created *phs1*Δ *htd2*Δ cells expressing human ceramide synthase CERS5. In these cells both yeast HACD homolog *PHS1* and the mitochondrial 3-OH acyl carrier protein dehydratase *HTD2* were deleted. Htd2 is a component of FA synthase type II (35). Because VLCFA production is essential for yeast growth, any genes involved in FA elongation, including *PHS1*, cannot be deleted under normal conditions (4). In yeast, most VLCFAs are used for sphingolipid synthesis, and the lethality of the VLCFA-deficient cells can be attributed to the loss of sphingolipid production due to the substrate specificity of yeast ceramide synthases. Therefore, genes of the FA elongation machinery can be deleted if yeast cells are engineered to produce ceramides/sphingolipids, such as by ectopic expression of the human ceramide synthase CERS5, which uses LCFAs for ceramide synthesis (36).

Phs1, HACD1, or HACD2 was expressed as triple FLAG (3xFLAG)-tagged protein in the *phs1*Δ *htd2*Δ/*CERS5* cells. Expression levels of HACD2 were the highest, and those of Phs1 were the lowest (Fig. 5*A*). Although the only commercially available 3-OH acyl-CoA species is 3-OH palmitoyl-CoA, several acyl-CoA species can be obtained. Therefore, we performed an *in vitro* FA elongation assay, in which [^{14}C]malonyl-CoA and acyl-CoA were used as substrates for the FA elongation cycle, instead of the 3-OH acyl-CoA dehydratase assay using a 3-OH acyl-CoA substrate. Membrane fractions were prepared from the yeast cells and were subjected to *in vitro* FA elongation assay using stearoyl-CoA (C18:0-CoA) as an acyl-CoA substrate. After the reactions, the products were converted to FA methyl esters (FAMEs), separated by reverse-phase TLC, and detected using autoradiography. In the control

*phs1*Δ *htd2*Δ/*CERS5* cells bearing the vector, C18:0-CoA was converted to 3-OH 20:0-CoA via 3-keto 20:0-CoA by endogenous FA elongases (Fen1 and Sur4) and 3-ketoacyl-CoA reductase Ifa38 (Fig. 5*B*). No further conversion was observed, due to the lack of 3-OH acyl-CoA dehydratase. When the *PHS1* gene was added back, the cells recovered the ability to produce C20:0- to C26:0-CoAs. Note that 3-ketoacyl-CoA and *trans*-2-enoyl-CoA intermediates were not observed in this assay, because the second and fourth reactions in the FA elongation cycle are rapid. Expression of HACD1 caused production of C20:0- to C26:0-CoAs as well, although their levels were lower than with Phs1 expression. Instead, more 3-OH acyl-CoA intermediates were accumulated. Expression of HACD2 resulted in production of C20:0- to C26:0-CoAs with similar efficiency to Phs1. The levels of 3-OH acyl-CoAs were higher than seen with Phs1, but lower than with HACD1. These results were assessed in more detail by LC-MS/MS using the stable isotope ^{13}C-labeled malonyl-CoA. Again, C20:0- to C26:0-CoAs were produced under expression of Phs1, HACD1, or HACD2, and 3-OH acyl-CoA levels were the highest in HACD1-expressing membranes (Fig. 5, *C* and *D*).

We also examined the activities of HACD1 and HACD2 in the monounsaturated FA elongation pathway using [^{13}C]malonyl-CoA and oleoyl-CoA (C18:1-CoA) as substrates. Expression of Phs1, HACD1, or HACD2 resulted in production of C20:1- to C26:1-CoAs (Fig. 5*E*). In most cases, the levels of the acyl-CoAs produced by HACD1- and HACD2-expressing membranes were slightly lower than those produced by Phs1-expressing membranes. The levels of 3-OH acyl-CoAs were higher in HACD1- and HACD2-expressing membranes than those in Phs1-expressing membranes, but there were no significant differences between those produced by HACD1- and HACD2-expressing membranes (Fig. 5*F*). Together with the results obtained from the FA elongation assay using C18:0-CoA, these results indicate that both HACD1 and HACD2 exhibit activities toward C20- to C26 saturated and monounsaturated 3-OH acyl-CoAs. However, the HACD1-mediated FA elongation cycle produces more saturated 3-OH acyl-CoA intermediates (but not monounsaturated 3-OH acyl-CoAs) than the HACD2-mediated cycle.

Broad and redundant substrate specificities of HACD1 and HACD2

Functions of HACD1 and HACD2 in the polyunsaturated FA elongation cycle could not be determined by the above yeast system, because yeast FA elongation machinery cannot elongate polyunsaturated acyl-CoAs. We therefore used a mammalian system, in which the *HACD* gene(s) were disrupted in the haploid human cell line HAP1 by CRISPR/Cas9 genome editing. Quantitative real-time RT-PCR analysis revealed that expression levels of *HACD3* mRNA were the highest in HAP1 cells, followed by *HACD1* and *HACD2* (Fig. 6*A*). No expression of *HACD4* was detected in HAP1 cells.

HACD1 KO, *HACD2* KO, *HACD3* KO, and *HACD1 HACD2* double KO (DKO) HAP1 cells were created. These cells were incubated with d_{31}-C16:0-COOH for 6 h. Lipids were then extracted and hydrolyzed to FAs by alkaline treatment, and d_{31}-labeled FAs were quantified by LC-MS/MS analysis. Almost no differences were observed in the compositions of d_{31}-labeled FAs between the control, *HACD1* KO, and *HACD3* KO cells (Fig. 6*B*). In contrast, ≥C18 saturated and monounsaturated FAs were reduced in *HACD2* KO cells, concomitant with increases in C16 FAs. The *HACD1 HACD2* DKO caused a greater decrease in C18:0 to C22:0 FAs and increase in C16 FAs than the *HACD2* single KO. Trace amounts of d_{31}-labeled ≥C18 saturated and monounsaturated FAs were still detected, even in the *HACD1 HACD2* DKO cells, suggesting that HACD3 or other unknown 3-OH acyl-CoA dehydratases produced them under the *HACD1* and *HACD2*-null conditions.

When cells were labeled with d_9-C18:1-COOH, similar results were obtained as with d_{31}-C16:0-COOH labeling. There was a decrease in ≥C20 monounsaturated FAs in *HACD2* KO cells and *HACD1 HACD2* DKO cells, whereas C18 monounsaturated FA was increased in these cells (Fig. 6*C*). d_{11}-C18:2(*n*-6)-COOH (Fig. 6*D*) and d_5-C18:3(*n*-3)-COOH (Fig. 6*E*) labeling experiments indicated that C20, C24, and C26 polyunsaturated FAs were decreased in *HACD2* KO cells relative to control cells, and further decreased in *HACD1 HACD2* DKO cells in most cases, whereas C18 polyunsaturated FAs were increased. The exception was C20:5(*n*-3)-COOH, which was slightly increased in *HACD2* KO cells relative to control cells (Fig. 6*E*). The levels of C20 polyunsaturated FAs are determined by the balance between the increase due to C18-to-C20 conversion and the decrease due to C20-to-C22 conversion. *HACD2* disruption appeared to have a stronger effect on C20-to-C22 polyunsaturated FA conversion than on C18-to-C20 polyunsaturated FA conversion, which might explain the slight increase in C20:5(*n*-3)-COOH levels in *HACD2* KO cells. Single gene disruption of *HACD1* or *HACD3* had almost no effect on polyunsaturated FA elongation (Fig. 6, *D* and *E*). Thus, HACD2 is the major 3-OH acyl-CoA dehydratase, not only for saturated and monounsaturated FA elongation, but also for polyunsaturated FA elongation, and HACD1 has a redundant function, albeit weaker than HACD2.

Weak activity of HACD3 in saturated and monounsaturated FA elongation pathways

HACD4 mRNA was not expressed in HAP1 cells (Fig. 6*A*). Therefore, we could not examine the activity of HACD4 via the above assay. Furthermore, the activity of HACD3 remained unclear, because the high activity of HACD2 might have masked the HACD3 activity. To circumvent these problems, each of the 3xFLAG-tagged HACDs was overproduced in *HACD1 HACD2* DKO cells. Expression of 3xFLAG-tagged HACD1–4 proteins was confirmed by immunoblotting (Fig. 7*A*). Cells were labeled with deuterium-labeled FAs (d_{31}-C16:0-COOH (Fig. 7*B*), d_9-C18:1-COOH (Fig. 7*C*), d_{11}-C18:2(*n*-6)-COOH (Fig. 7*D*), and d_5-C18:3(*n*-3)-COOH (Fig. 7*E*)). Replacing *HACD1* or *HACD2* into *HACD1 HACD2* DKO cells reversed the decreased levels of FA elongation products and increased substrate FA levels (Fig. 7, *B*–*E*). Expression of HACD3 had a slight effect on the elongation of saturated and monounsaturated FAs but had few effects on that of polyunsaturated FAs. In the d_{31}-C16:0-COOH labeling experiment, C18:0-COOH and C18:1-COOH were increased relative to the control, but C16:0-COOH was decreased (Fig. 7*B*). Similarly, in the

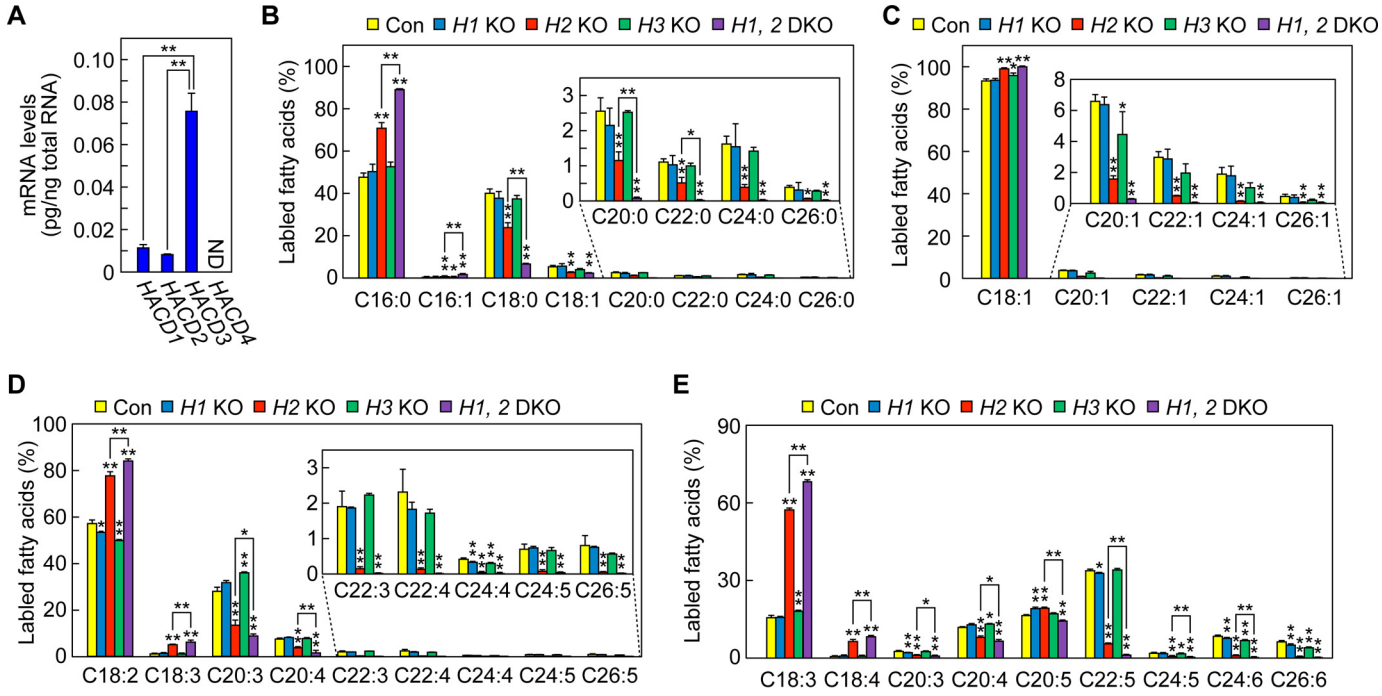

Figure 6. HACD2 is the major 3-OH acyl-CoA dehydratase in HAP1 cells. *A*, total RNAs prepared from HAP1 cells were subjected to SYBR Green-based real-time quantitative RT-PCR using specific primers for *HACD1*, *HACD2*, *HACD3*, and *HACD4*. Absolute values of the mRNA levels were calculated by comparison with the levels of the PCR products amplified from the corresponding plasmid encoding *HACD1*, *HACD2*, *HACD3*, or *HACD4*. Values represent the means ± S.D. from three independent reactions. Statistically significant differences are represented (**, $p < 0.01$; Tukey's test). *ND*, not detected. *B–E*, WT (control), *HACD1* KO, *HACD2* KO, and *HACD1 HACD2* DKO HAP1 cells were treated with 1 μM d_{31}-palmitic acid (*B*), d_9-oleic acid (*C*), d_{11}-linoleic acid (*D*), or d_5-α-linolenic acid (*E*) for 6 h (*B* and *E*), 2 h (*C*), or 4 h (*D*) at 37 °C. Lipids were extracted, saponified, derivatized to AMPP amides, and analyzed by LC-MS/MS. Values are the means ± S.D. of the quantities of deuterium-labeled FAs with the indicated chain length and desaturation number from three independent experiments. Statistically significant differences are calculated by Tukey's test (**, $p < 0.01$; *, $p < 0.05$). Of the significant differences found, only those from the control (without lines connecting the bar graphs) and those between *HACD2* KO and *HACD1 HACD2* DKO (with lines connecting the bar graphs) are represented. *Con,* control; *H*, *HACD*.

d_9-C18:1-COOH labeling experiment, C20:1-COOH and C22:1-COOH were increased relative to the control, but C18:1-COOH was decreased (Fig. 7*C*). No effect on FA elongation was observed for HACD4 overexpression, irrespective of FA species (Fig. 7, *B–E*). These results indicate that HACD3 exhibits weak activity toward saturated and monounsaturated 3-OH acyl-CoAs but that HACD4 exhibits no such activity.

Discussion

In the FA elongation cycle in mammals, there are multiple isozymes able to catalyze the first step, condensation (ELOVL1–7), and the third step, dehydration (HACD1–4). Although knowledge relating to the differences in the substrate specificities and physiological functions of the ELOVLs has been accumulated (6, 7, 11, 22), such information was limited for HACD1–4. Although it was known that HACD1–4 exhibits activities toward 3-OH palmitoyl-CoA *in vitro* (26), their activities toward other 3-OH acyl-CoA species, as well as their actual activities within cells, had not been determined.

ELOVL1–7 exhibit characteristic substrate specificities: ELOVL1, saturated and monounsaturated C20- to C24-CoAs; ELOVL2, polyunsaturated C20- to C22-CoAs; ELOVL3, C16- to C22-CoAs; ELOVL4, ≥C24-CoAs; ELOVL5, polyunsaturated C18- and C20-CoAs; ELOVL6, saturated and monounsaturated C12- to C16-CoAs; and ELOVL7, C16- to C20-CoAs (6, 7, 11, 22, 37). This study revealed that, in contrast to the ELOVLs, the substrate preferences of HACD1 and HACD2 are quite broad; both were active in all steps of the FA elongation pathways of saturated, monounsaturated, and *n*-6 and *n*-3 polyunsaturated FAs (Figs. 5–7). In mouse skeletal muscle, the expression levels of *HACD1* mRNA were much higher (~75-fold) than those of *HACD2* mRNA (Fig. 3*A*). However, 3-OH acyl-CoA dehydratase activity toward 3-OH palmitoyl-CoA in *Hacd1* KO skeletal muscle was reduced only moderately (to ~60% of the control), and the compositions of the membrane lipids and metabolism of exogenously added FAs were unchanged (Figs. 3 and 4). It is likely that HACD2 was responsible for the remaining activity in *Hacd1* KO muscle. In HAP1 cells, HACD2 was the predominant 3-OH acyl-CoA dehydratase over HACD1 (Fig. 6, *B–E*), although the expression levels of *HACD2* mRNA were 71% of those of *HACD1* mRNA (Fig. 6*A*). Together with the ubiquitous tissue distribution of *HACD2* (27), these results suggest that HACD2 is the major 3-OH acyl-CoA dehydratase in the whole body.

The need for HACD1 is unclear, because HACD2 has the same function as and higher activity levels than HACD1. The only difference that we observed between HACD1 and HACD2 in this study was in the levels of saturated 3-OH acyl-CoA intermediates during the FA elongation process; 3-OH acyl-CoAs were accumulated at higher levels in HACD1-expressing membranes than in HACD2-expressing membranes (Fig. 5, *B* and *D*). In the FA elongation assay, acyl-CoAs are the main detectable products, although 3-OH acyl-CoAs are also detected at

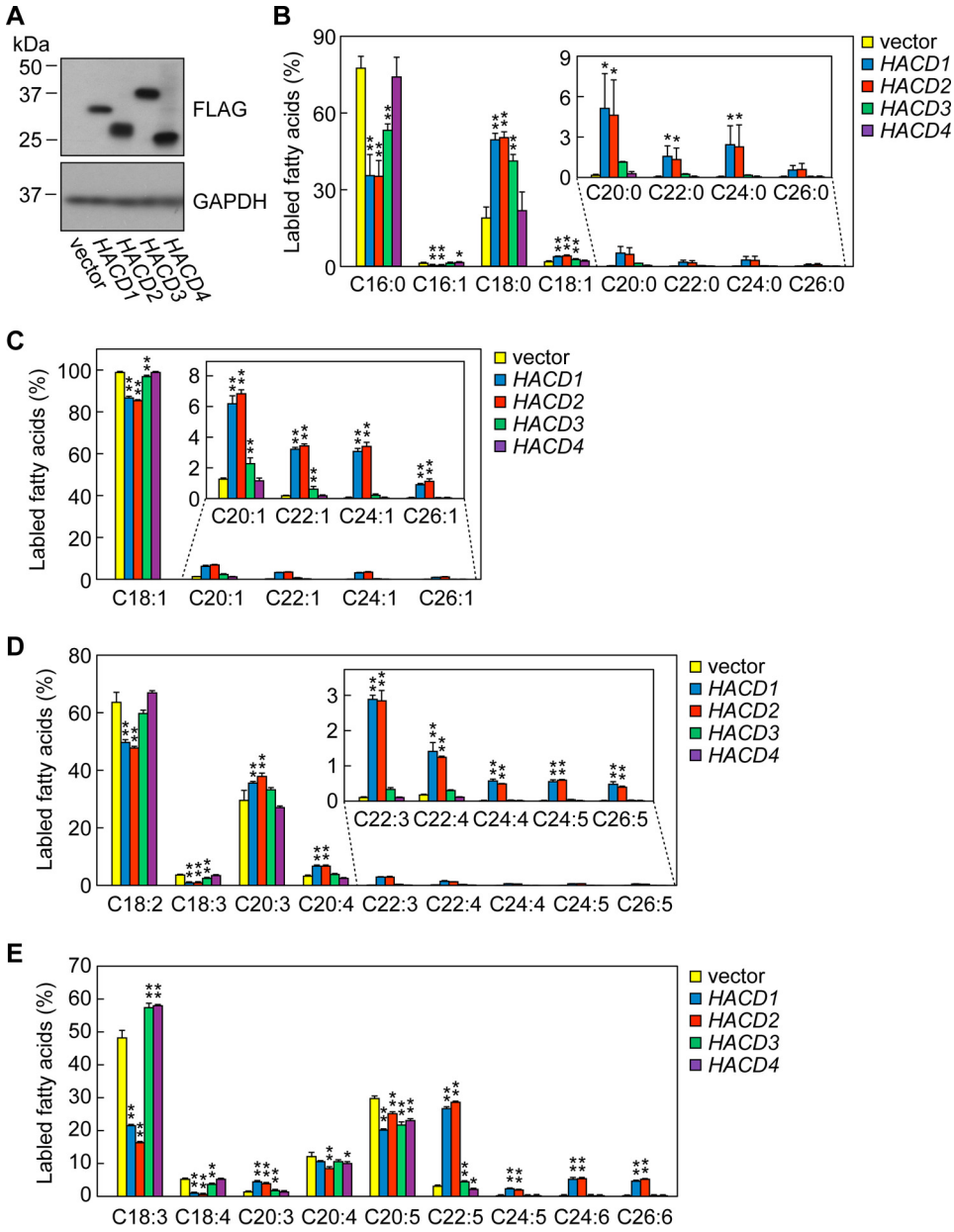

Figure 7. Redundancy and broad substrate preferences of HACD1 and HACD2. *A–E*, *HACD1 HACD2* DKO HAP1 cells were transfected with the pCE-puro 3xFLAG-1 (vector), pCE-puro 3xFLAG-HACD1, pCE-puro 3xFLAG-HACD2, pCE-puro 3xFLAG-HACD3, or pCE-puro 3xFLAG-HACD4 plasmid. Twenty-four hours after transfection, 2 μg/ml puromycin was added to the culture medium to kill the non-transfected cells, and the culture was incubated for a further 24 h. Cells were then treated with 1 μM d_{31}-palmitic acid (*A* and *B*), d_9-oleic acid (*C*), d_{11}-linoleic acid (*D*), or d_5-α-linolenic acid (*E*) for 24 h at 37 °C. *A*, proteins (10 μg) were prepared, separated by SDS-PAGE, and detected by immunoblotting with anti-FLAG and anti-GAPDH (loading control) antibodies. *B–E*, lipids were extracted, saponified, derivatized to AMPP amides, and analyzed by LC-MS/MS. Values are the means ± S.D. of the quantities of deuterium-labeled FAs with the indicated chain length and desaturation number from three independent experiments. Statistically significant differences from the control are represented (**, $p < 0.01$; *, $p < 0.05$; Dunnett's test).

low levels (38). This indicates that the first (condensation) step catalyzed by ELOVLs is rate-limiting, and the third (dehydration) step catalyzed by HACDs is secondarily rate-limiting in the FA elongation cycle. Neither 3-ketoacyl-CoAs nor *trans*-2-enoyl-CoAs are detected under normal conditions (38), indicating that the second step, catalyzed by KAR, and the fourth step, catalyzed by TECR, are rapid. These fast reactions seem to be achieved by the interplays between the ELOVLs and KAR as well as those between the HACDs and TECR, which enable direct transfer of the FA elongation cycle intermediates from the ELOVLs/HACDs to KAR/TECR without release from the FA elongation machinery (38, 39). However, the detection of 3-OH acyl-CoA intermediates in the FA elongation cycle (Fig. 5) (38) implies that some 3-OH acyl-CoAs are released from the FA elongation machinery and used for other purposes. We hypothesize that 3-OH acyl-CoAs or their derivatives have certain regulatory functions in skeletal muscle, such as cell growth, differentiation, and fusion, and that this may explain the high levels of HACD1 in skeletal muscle.

Mutations in *HACD1* cause myopathy in humans and dogs (29, 30). *Hacd1* disruption also causes a myopathic phenotype in mice (31), although the molecular mechanism remains

largely unclear. We also observed decreased body size, body weight, and skeletal muscle weight in *Hacd1* KO mice (Fig. 2, *C–E*). Because HACD1 is involved in FA elongation, it had been hypothesized that membrane lipid compositions, especially those of longer lipids, might be affected by *Hacd1* disruption in skeletal muscle. However, we could not detect any differences in the compositions of membrane lipids (Fig. 3, *D–F*). This suggests that certain changes in lipid composition may occur during the developmental stages, such as the mesoderm to muscle or myoblast to myofiber differentiation stages.

Although the expression levels of *HACD3* mRNA were the highest among the *HACDs* in HAP1 cells, gene disruption of *HACD3* had no effect on FA elongation (Fig. 6). The activity of HACD3 toward saturated and monounsaturated 3-OH acyl-CoAs was only detected when it was overproduced in *HACD1 HACD2* DKO cells (Fig. 7). In this study, no HACD4 activity was detected. To date, HACD4 activity toward 3-OH C16:0-CoA has only been detected *in vitro* when HACD4 was solubilized with the nonionic detergent Triton X-100, although the V_{max} value was the lowest among the HACDs (26). In the cell-based assay performed in this study, we examined the activity of HACD4 toward 3-OH acyl-CoAs with ≥C18, but not toward that with C16, in the saturated FA elongation pathway. Considering the low and zero activity of HACD3 and HACD4, respectively, in the cell-based assay, we hypothesize that their natural substrates are not 3-OH acyl-CoAs with ≥C18 but rather are specialized forms of 3-OH acyl-CoAs, such as those containing a short or branched chain. Because HACD4 is expressed specifically in leukocytes (26), it is possible that it functions in the metabolism of pathogen-derived 3-OH short FAs. For example, the lipid A portion of lipopolysaccharides of the Gram-negative bacteria *E. coli* contains 3-OH C14:0-COOH (40). Further studies are needed, however, to elucidate the physiological functions and exact substrates of HACD3 and HACD4.

Experimental procedures

Generation of Hacd1$^{-/-}$ mice

The *Hacd1* KO targeting vector contains the upstream region (~7,000 bp) of exon 6, the *Pgk-neo* (neomycin-resistant gene under the control of the *Pgk* promoter) cassette flanked by two *loxP* sequences, the downstream region (~2,000 bp) of exon 6, and the *Tk-DTA* (diphtheria toxin A under the control of thymidine kinase promoter) cassette (Fig. 2*A*). The targeting vector was constructed using the recombineering method (41) with the bacterial artificial chromosome clone bMQ-431D1 (BACPAC Resources Center; Oakland, CA) prepared from chromosomal DNAs of *Mus musculus* AB2.2 (129S7/SvEvBrd-Hprtb-m2) in ES cells (42). After transfection of the linearized targeting vector into E14 ES cells, G418-resistant clones were selected. Genomic DNAs were prepared from each clone, and homologous recombination was confirmed by genomic PCR using primers p1 and p2 (Table 1 and Fig. 2*A*). Recombination was also confirmed by Southern blotting. Positive ES clones were injected into C57BL/6J blastocysts, and the resulting chimera mice were crossed with C57BL/6J mice to obtain *Hacd1*$^{+/-}$ mice. After crossing *Hacd1*$^{+/-}$ mice with C57BL/6J mice repeatedly (≥10 generations of back-crossing), *Hacd1*$^{-/-}$ mice were generated by intercrossing the *Hacd1*$^{+/-}$ mice. Genotyping was performed by PCR using genomic DNAs and primers p3 and p2 for detection of the *Hacd1* WT allele and p1 and p2 for detection of the *Hacd1* KO allele (Table 1 and Fig. 2*A*). All mice were kept at 23 ± 1 °C in a 12-h light/dark cycle with a standard chow diet (PicoLab Rodent Diet 20; LabDiet, St. Louis, MO) and water available *ad libitum*. The animal experiments performed in this study were approved by the institutional animal care and use committees of Hokkaido University and RIKEN Brain Science Institute.

Table 1
Nucleotide sequences of primers used in this study

Primer	Nucleotide sequence
p1	5′-CATGCTCCAGACTGCCTTGGGAAAAGC-3′
p2	5′-CCTTGCGGGTGTCAGGCGACTCCGC-3′
p3	5′-CAAGTATTTGGAATAGCAAGGGAAGC-3′
mHacd1-F	5′-ATGGCGTCCAGTGAGGAGGACGGC-3′
mHacd1-R	5′-TTAATCGTCCTTCTCCGCGATC-3′
mHacd2-F	5′-TGCTATAGGGATTGTGCCATC-3′
mHacd2-R	5′-ACGGATAATTTCCGTGATTGTCC-3′
mHacd3-F	5′-GACGTGCAGAACCCTGCTATC-3′
mHacd3-R	5′-CTTCTGGACTGTGATGTTCACC-3′
mHacd4-F	5′-CAGCTCACAGAGAGAGTGATC-3′
mHacd4-R	5′-GAGTGTTTGACTGAGCCATGTC-3′
mGapdh-F	5′-TGAAGGTCGGTGTCAACGGATTTGGC-3′
mGapdh-R	5′-CATGTAGGCCATGAGGTCCACCAC-3′
hHACD1-F	5′-TGGTGTGGCTCATTACTCACAG-3′
hHACD1-R	5′-TGGCAAGTGGTCAAGAAGGC-3′
hHACD2-F	5′-TGGGCAGTAACACATAGCGTC-3′
hHACD2-R	5′-ACCTGGCCCATTTGATGAGG-3′
hHACD3-F	5′-GCGACCACTGTTTTTGGCTC-3′
hHACD3-R	5′-AGAGCCTTCGCTTTCCAGTC-3′
hHACD4-F	5′-CAGTTCTGTGGCCACTCTTG-3′
hHACD4-R	5′-GATGCGACTTTGCCAATCCG-3′
HACD1-CC1-F2	5′-GGTCATGGCGATGTCGTAGAGTTTT-3′
HACD1-CC1-R2	5′-TCTACGACATCGCCATGACCCGGTG-3′
HACD1-CC1-F3	5′-CTCGGGCCCTCCCCGCGCCGGTTTT-3′
HACD1-CC1-R3	5′-CGGCGCGGGGAGGGCCCGAGCGGTG-3′
HACD2-CC1-F1	5′-ACGCCGTGGCCAGGGGCCCCGTTTT-3′
HACD2-CC1-R1	5′-GGGGCCCCTGGCCACGGCGTCGGTG-3′
HACD2-CC1-F2	5′-TACAATGTGGTGATGACAGCGTTTT-3′
HACD2-CC1-R2	5′-GCTGTCATCACCACATTGTACGGTG-3′
HACD3-CC2-F1	5′-AAGTCAGGAGCCAAAAACAGGTTTT-3′
HACD3-CC2-R1	5′-CTGTTTTTGGCTCCTGACTTCGGTG-3′
HACD3-CC2-F2	5′-GGATGAATCTGATGCGGAAAGTTTT-3′
HACD3-CC2-R2	5′-TTTCCGCATCAGATTCATCCCGGTG-3′

Plasmids

The pAK1018 and pAK440 vectors are derivatives of the pRS426 yeast expression vector (*URA3* marker, 2 μ origin), designed to produce an N-terminal tandemly oriented His_6, Myc epitope, and a triple FLAG (HMF)-tagged protein under the glyceraldehyde-3-phosphate dehydrogenase (GAPDH: *TDH3*) promoter and a C-terminal 3xFLAG-tagged protein, respectively. The pRF6 (*PHS1–3xFLAG*) plasmid was constructed by cloning the *PHS1* gene, together with its promoter, into the pAK440 vector. The pYS10 (*HMF-HACD1*) and pTN28 (*HMF-HACD2*) plasmids were constructed by cloning human *HACD1* and *HACD2* into the pAK1018 plasmid, respectively. The pCE-puro 3xFLAG-1 plasmid is a mammalian expression vector, designed to produce an N-terminally 3xFLAG-tagged protein under the human elongation factor 1α promoter (43). The pCE-puro 3xFLAG-HACD1, pCE-puro 3xFLAG-HACD2, pCE-puro 3xFLAG-HACD3, and pCE-puro 3xFLAG-HACD4 plasmids are derivatives of the pCE-puro 3xFLAG-1 vector and were described previously (26).

The all-in-one CRISPR/Cas9 vector pYU417, which consists of a *Cas9* D10A mutant nuclease (*Cas9* nickase), a guide RNA cloning cassette, *EGFP*, and puromycin *N*-acetyltransferase gene, was constructed from the GeneArt CRISPR Nuclease Vector with the OFP plasmid (Thermo Fisher Scientific, Waltham, MA) by introducing D10A mutation into the *Cas9* nuclease, incorporating puromycin *N*-acetyltransferase gene, and substituting the *ORF* reporter with *EGFP*. Each forward (-F) and reverse (-R) primer set for guide RNA expression (for *HACD1* KO, HACD1-CC1-F2, HACD1-CC1-R2, HACD1-CC1-F3, and HACD1-CC1-R3; for *HACD2* KO, HACD2-CC1-F1, HACD2-CC1-R1, HACD2-CC1-F2, and HACD2-CC1-R2; for *HACD3* KO, HACD3-CC2-F1, HACD3-CC2-R1, HACD3-CC2-F2, and HACD3-CC2-R2; Table 1) was annealed and inserted into the pYU417 vector, generating pYU-HACD1-CC1-2, pYU-HACD1-CC1-3, pYU-HACD2-CC1-1, pYU-HACD2-CC1-2, pYU-HACD3-CC2-1, and pYU-HACD3-CC2-2 plasmids. The all-in-one CRISPR/Cas9 plasmid (pX330A-puro-HACD1/HACD2) for *HACD1 HACD2* DKO was constructed using the pX330A-puro-1x4, pX330S-puro-2, pX330S-puro-3, and pX330S-puro-4 vectors in the Multiplex CRISPR/Cas9 Assembly System kit (Addgene, Cambridge, MA) as described previously (44, 45). The primers used for the construction were HACD2-CC1-F1, HACD2-CC1-R1, HACD2-CC1-F2, HACD2-CC1-R2, HACD1-CC1-F2, HACD1-CC1-R2, HACD1-CC1-F3, and HACD1-CC1-R3 (Table 1).

Yeast strains and media

The yeast *S. cerevisiae* strains BY4741 (*MAT**a** his3*Δ*1 leu2*Δ*0 met15*Δ*0 ura3*Δ*0*) and 6615 (BY4741, *htd2*Δ*::KanMX4*) were described previously (46, 47). KMY81 (*phs1*Δ*::LEU2 htd2*Δ*::KanMX4*/pAB119 (*3xFLAG-CERS5*, *HIS3* marker)) was constructed by deletion of the *PHS1* gene in the yeast strain 6615 bearing the pAB119 plasmid (36), using a *phs1*Δ*::LEU2* fragment by homologous recombination. Cells were grown in synthetic complete medium (0.67% yeast nitrogen base, 2% D-glucose, and nutritional supplements), but without histidine and uracil, at 30 °C.

In vitro 3-OH acyl-CoA dehydratase assay

Total cell lysates were prepared from mouse gastrocnemius by homogenizing the tissues, using a homogenizer, in buffer A (50 mM HEPES/NaOH (pH 7.5), 150 mM NaCl, 10% glycerol, 1× protease inhibitor mixture (Complete, EDTA-free; Roche Diagnostics, Basel, Switzerland), 1 mM PMSF, and 1 mM DTT), followed by sonication and removal of cell debris by centrifugation (400 × *g*, 3 min, 4 °C). They were then subjected to centrifugation at 100,000 × *g* for 30 min at 4 °C, and the resulting pellet (total membrane fraction) was suspended in buffer A. The *in vitro* 3-OH acyl-CoA assay was performed as described previously (32) in reaction buffer I (total volume of 50 μl; buffer A containing 1 mM $CaCl_2$, 2 mM $MgCl_2$, and 0.1% digitonin). The total membrane fractions (20 μg of protein) were incubated with 0.01 μCi of [^{14}C]3-OH palmitoyl-CoA (55 mCi/mmol; American Radiolabeled Chemicals, St. Louis, MO) for 10 min at 37 °C. After terminating the reactions by adding 25 μl of 75% KOH (w/v) and 50 μl of ethanol, the lipids were saponified for 1 h at 70 °C. Samples were then acidified by adding 100 μl of 5 M HCl and 50 μl of ethanol. Lipids were extracted with 700 μl of hexane, dried, suspended in 20 μl of chloroform, separated by TLC on Silica Gel 60 high performance TLC plates (Merck, Darmstadt, Germany) with hexane/diethyl ether/acetic acid (30:70:1, v/v) as the solvent system, and detected using a BAS-2500 image analyzer (GE Healthcare, Little Chalfont, UK).

Real-time quantitative RT-PCR

Total RNAs were isolated using the NucleoSpin RNA II kit (Takara Bio, Shiga, Japan) and then converted to cDNA using the PrimeScript II 1st strand cDNA Synthesis kit (Takara Bio), both according to the manufacturer's instructions. Real-time quantitative PCR was performed using KOD SYBR qPCR mix (Toyobo, Osaka, Japan) and primers (mouse *Hacd1*, mHacd1-F and mHacd1-R; mouse *Hacd2*, mHacd2-F and mHacd2-R; mouse *Hacd3*, mHacd3-F and mHacd3-R; mouse *Hacd4*, mHacd4-F and mHacd4-R; mouse *Gapdh*, mGapdh-F and mGapdh-R; human *HACD1*, hHACD1-F and hHACD1-R; human *HACD2*, hHACD2-F and hHACD2-R; human *HACD3*, hHACD3-F and hHACD3-R; and human *HACD4*, hHACD4-F and hHACD4-R; Table 1) on a CFX96 Touch Real-time PCR Detection System (Bio-Rad), according to the manufacturer's manual.

LC-MS/MS analysis

Mouse gastrocnemius muscles (16 mg) were chopped and suspended in 144 μl of $CHCl_3$/MeOH/formic acid (100:200:1, v/v). Lipids were extracted by mixing samples vigorously in tubes containing zirconia beads for 1 min at 4 °C using Micro Smash MS-100 (TOMY Seiko, Tokyo, Japan). After centrifugation (1,000 × *g*, 10 min, 4 °C), the supernatant was mixed with 48 μl of chloroform and 86.4 μl of water, successively, with vigorous mixing. Phases were separated by centrifugation (9,100 × *g*, 1 min, room temperature), and the organic phase was recovered and dried. Lipids were dissolved in 100 μl of methanol for LC-MS/MS analysis.

LC-MS/MS analyses were performed as described previously (20, 45). Lipids were resolved and detected by ultra-performance LC on a reverse-phase column (ACQUITY UPLC CSH C18 column, length 100 mm; Waters) coupled with electrospray ionization tandem triple quadrupole MS (Xevo TQ-S, Waters). The conditions of ultra-performance LC and MS were as follows: temperature, 55 °C; flow rate, 0.4 ml/min; binary gradient system with mobile phase A (acetonitrile/water (3:2, v/v) containing 10 mM ammonium formate) and mobile phase B (acetonitrile/2-propanol (9:1, v/v) containing 10 mM ammonium formate); elution gradient steps, 0 min, 10% B; 0–6 min, gradient to 40% B; 6–15 min, gradient to 70% B; 15–18 min, gradient to 100% B; 18–23 min, 100% B; 23–23.1 min, gradient to 10% B; 23.1–25 min, 10% B; with electrospray ionization capillary voltage, 3.0 kV; sampling cone, 30 V; and source offset, 50 V for positive ion mode (for sphingomyelin and FAs) or capillary voltage, 2.0 kV; sampling cone, 30 V; and source offset, 30 V for negative ion mode (for phosphatidylcholine and phosphatidylinositol). Lipid detection was performed via multiple reaction monitoring, by selecting specific *m/z* for the quadrupole mass filters Q1 and Q3 (Tables 2–6). MassLynx software (Waters) was used for data analyses and quantification.

Table 2
Selected *m/z* values for sphingomyelin species in LC-MS/MS analysis

FA chain length	Precursor ion (Q1)[a]	Product ion (Q3)	Collision energy
			eV
C16:0	703.40	184.10	60
C18:0	731.40	184.10	60
C18:1	729.40	184.10	60
C20:0	759.40	184.10	60
C22:0	787.50	184.10	60
C24:0	815.60	184.10	60
C24:1	813.60	184.10	60

[a] Precursor ion is $[M + H]^+$.

Immunoblotting

Immunoblotting was performed as described previously (48). Anti-FLAG M2 antibody (1 μg/ml; Agilent Technologies, Santa Clara, CA), anti-Pma1 antibody (1:2,000 dilution; Thermo Fisher Scientific), or anti-GAPDH antibody (1:2,000 dilution; Thermo Fisher Scientific) was used as a primary antibody. Horseradish peroxidase-conjugated anti-mouse IgG $F(ab')_2$ fragment (1:7,500 dilution; GE Healthcare) was used as a secondary antibody. The chemiluminescence signal was detected using Western Lightning Plus-ECL (PerkinElmer Life Sciences, Waltham, MA) or Pierce ECL Western blotting Substrate (Thermo Fisher Scientific).

FA elongation assay

Total membrane fractions were prepared from yeast as described previously (49). FA elongation assay using [^{14}C]malonyl-CoA was performed as described previously (11, 12). Briefly, total membrane fractions (20 μg of protein) were incubated with 20 μM stearoyl-CoA (Sigma) complexed with 0.2 mg/ml FA-free bovine serum albumin (Sigma) and 75 nCi of [^{14}C]malonyl-CoA (American Radiolabeled Chemicals) in reaction buffer II (50 mM HEPES/NaOH (pH 6.8), 150 mM NaCl, 10% glycerol, 1× protease inhibitor mixture, 1 mM PMSF, 1 mM DTT, 2 mM $MgCl_2$, and 1 mM $CaCl_2$) containing the FA synthase inhibitor cerulenin (200 μg/ml; Sigma) and 1 mM NADPH. After the reaction, lipids were saponified, acidified, extracted, dried, and converted to FAMEs as described previously (11). FAMEs were extracted, dried, suspended in 20 μl of chloroform, separated by reverse-phase TLC (Silica Gel 60 RP-18 F_{254}s TLC plates; Merck) with chloroform/methanol/water (15:30:2, v/v), and detected using a BAS-2500 image analyzer.

FA elongation assay using [^{13}C]malonyl-CoA was performed as follows. Total membrane fractions (20 μg of protein) were incubated with 100 μM [^{13}C]malonyl-CoA (Sigma) and 10 μM acyl-CoA (stearoyl-CoA or oleoyl-CoA; Avanti Polar Lipids, Alabaster, AL) complexed with 0.2 mg/ml FA-free bovine serum albumin in 50 μl of reaction buffer III (50 mM HEPES/NaOH (pH 7.5), 150 mM NaCl, 10% glycerol, 1× protease inhibitor mixture, 1 mM PMSF, 1 mM DTT, 2 mM $MgCl_2$, and 1 mM $CaCl_2$) containing 200 μg/ml cerulenin and 1 mM NADPH for 30 min at 30 °C. The reactions were terminated by adding 25 μl of 75% KOH (w/v) and 50 μl of ethanol, then saponified for 1 h at 70 °C, and acidified by adding 100 μl of 5 M formic acid with 50 μl of ethanol. Lipids were extracted with 750 μl of hexane and dried. FAs were derivatized to AMPP amides using the AMP$^+$ mass spectrometry kit (Cayman Chemical, Ann Arbor, MI), according to the manufacturer's protocol, and resolved by LC-MS/MS as described above.

Table 3
Selected *m/z* values for phosphatidylcholine species in LC-MS/MS analysis

FA chain lengths (*sn*-1 and *sn*-2)	Precursor ion (Q1)[a]	Product ion (Q3)	Collision energy
			eV
C14:0/C16:0	750.40	227.00	50
C14:0/C18:1	776.40	227.00	50
C16:1/C16:1	774.40	253.00	50
C16:0/C16:0	778.40	255.00	50
C16:0/C18:2	802.40	255.00	50
C16:1/C18:1	802.40	253.00	50
C16:0/C18:1	804.40	255.00	50
C16:0/C18:0	806.40	255.00	50
C16:0/C20:4	826.40	255.00	50
C18:1/C18:3	826.40	277.00	50
C18:2/C18:2	826.40	279.00	50
C18:1/C18:2	828.40	281.00	50
C18:1/C18:1	830.40	281.00	50
C18:0/C18:2	830.40	283.00	50
C18:0/C18:1	832.40	283.00	50
C16:0/C22:6	850.40	255.00	50
C18:0/C20:4	854.00	283.00	50
C18:0/C22:6	878.40	283.00	50

[a] Precursor ion is $[M + HCOO]^-$.

Table 4
Selected *m/z* values for phosphatidylinositol species in LC-MS/MS analysis

FA chain lengths (*sn*-1 and *sn*-2)	Precursor ion (Q1)[a]	Product ion (Q3)	Collision energy
			eV
C16:1/C16:1	805.30	253.00	60
C18:0/C16:1	835.40	283.00	60
C18:0/C16:0	837.40	283.00	60
C16:0/C20:4	857.30	255.00	60
C18:1/C18:1	861.40	281.00	60
C18:0/C18:2	861.00	283.00	60
C18:1/C20:4	883.40	281.00	60
C18:0/C20:4	885.40	283.00	60
C18:0/C20:3	887.40	283.00	60
C18:0/C22:6	909.40	283.00	60
C18:0/C22:5	911.40	283.00	60
C18:0/C22:4	913.40	283.00	60

[a] Precursor ion is $[M - H]^-$.

Cell culture

HAP1 is a near-haploid human cell line derived from myelogenous leukemia (50) and was purchased from the American Type Culture Collection (Manassas, VA). HAP1 cells were grown in Iscove's modified Dulbecco's medium (12440-053; Thermo Fisher Scientific) containing 10% FBS, 100 units/ml penicillin, and 100 μg/ml streptomycin. Transfections were performed using Lipofectamine Plus Reagent (Thermo Fisher Scientific), according to the manufacturer's instruction. The transfected cells were subjected to selection in 2 μg/ml puromycin for 2 days.

Mouse primary cultured myoblasts were prepared essentially as described previously (51). The gastrocnemius, tibialis anterior muscles, and thigh muscles were collected from the hindlimbs of the 1-month-old mice, shredded in PBS, and incubated with 5 ml of cell separation solution I (DMEM (D6429; Sigma) containing 10% FBS and 1.4 units/ml collagenase D (Roche Diagnostics)) for 1 h at 37 °C. The muscle cells were then disaggregated by passing them through a syringe with an

Table 5
Selected *m/z* values for [^{13}C]malonyl-CoA metabolites in LC-MS/MS analysis

FA chain length	Precursor ion (Q1)[a]	Product ion (Q3)	Collision energy
			eV
C13:0	381.10	238.90	55
[^{13}C]3-OH C20:0	497.10	229.08	55
[^{13}C]C20:0	481.10	240.90	55
[^{13}C]3-OH C22:0	527.10	229.08	55
[^{13}C]C22:0	511.10	241.90	55
[^{13}C]3-OH C24:0	557.20	229.08	55
[^{13}C]C24:0	541.20	241.90	55
[^{13}C]3-OH C26:0	587.20	229.08	55
[^{13}C]C26:0	571.20	241.90	55
[^{13}C]3-OH C20:1	495.10	229.08	55
[^{13}C]C20:1	479.10	240.90	55
[^{13}C]3-OH C22:1	525.10	229.08	55
[^{13}C]C22:1	509.10	241.90	55
[^{13}C]3-OH C24:1	555.10	229.08	55
[^{13}C]C24:1	539.10	241.90	55
[^{13}C]3-OH C26:1	585.10	229.08	55
[^{13}C]C26:1	569.10	241.90	55

[a] Precursor ion is $[M + H]^+$.

18-gauge needle and centrifuged (650 × *g*, 3 min, room temperature). The resulting pellets were suspended in 5 ml of cell separating solution II (DMEM containing 10% FBS, 1.4 units/ml collagenase D, and 1.5 units/ml dispase (Thermo Fisher Scientific)), incubated for 30 min at 37 °C, and then passed through a syringe with an 18-gauge needle. The cell solution was filtered using a 70-μm cell strainer (Corning) and a 35-μm cell strainer (Corning). The mouse primary cultured myoblasts thus obtained were grown in F-10 medium (Thermo Fisher Scientific) containing 20% FBS, 100 units/ml penicillin, 100 μg/ml streptomycin (Sigma), and 5 ng/ml basic fibroblast growth factor (PeproTech, Rocky Hill, NJ). Cells were cultured in dishes coated with Matrigel (Corning) diluted 10-fold with DMEM. Differentiation into myotube cells was induced by replacing the medium with Skeletal Muscle Cell Differentiation Medium (Takara Bio), and the cells were cultured.

Lipid labeling assay

Cells were incubated with 1 μM deuterium-labeled FA (d_{31}-palmitic acid (Cayman Chemical), d_9-oleic acid (Avanti Polar Lipids), d_{11}-linoleic acid (Cayman Chemical), or d_5-α-linolenic acid (Cayman Chemical), where d_{31} means that the FA contained 31 deuteriums) for 24 h at 37 °C. Cells were then washed with PBS, detached from the dish by incubating them in 0.05% trypsin/EDTA solution, and resuspended in 100 μl of water. Lipids were extracted by mixing with successive additions of 375 μl of chloroform/methanol/formic acid (100:200:1, v/v), 125 μl of chloroform, and 125 μl of water. Phases were then separated by centrifugation, and the organic phase was recovered and treated with 71 μl of 0.5 M NaOH to hydrolyze the ester bonds (release FAs from lipids) for 1 h at 37 °C. After neutralization with 35.5 μl of 1 M formic acid, lipids were extracted via successive additions of 175 μl of chloroform and 250 μl of water with mixing. Phases were separated by centrifugation, and the organic phase was recovered, dried, derivatized with an AMP^+ mass spectrometry kit, and resolved by LC-MS/MS as described above.

Table 6
Selected *m/z* values for the metabolites of deuterium-labeled FAs in LC-MS/MS analysis

FA chain length	Precursor ion (Q1)[a]	Product ion (Q3)	Collision energy
			eV
d_{31}-C16:0	454.60	242.05	55
d_{31}-C16:1	450.60	242.05	55
d_{31}-C18:0	482.60	239.05	55
d_{31}-C18:1	478.60	239.05	55
d_{31}-C20:0	510.60	239.05	55
d_{31}-C22:0	538.60	239.05	55
d_{31}-C24:0	566.60	239.05	55
d_{31}-C26:0	594.60	239.05	55
d_9-C18:1	458.50	239.03	48
d_9-C20:1	486.50	239.03	48
d_9-C22:1	514.50	239.03	48
d_9-C24:1	542.50	239.03	48
d_9-C26:1	580.50	239.03	48
d_{11}-C18:2(*n*-6)	458.30	239.03	44
d_{11}-C18:3(*n*-6)	456.30	239.03	44
d_{11}-C20:3(*n*-6)	484.30	239.03	44
d_{11}-C20:4(*n*-6)	482.30	239.03	44
d_{11}-C22:3(*n*-6)	512.30	239.03	44
d_{11}-C22:4(*n*-6)	510.30	239.03	44
d_{11}-C24:4(*n*-6)	538.30	239.03	44
d_{11}-C24:5(*n*-6)	536.30	239.03	44
d_{11}-C26:5(*n*-6)	564.30	239.03	44
d_5-C18:3(*n*-3)	450.00	239.04	43
d_5-C18:4(*n*-3)	448.00	239.04	43
d_5-C20:3(*n*-3)	478.00	239.04	43
d_5-C20:4(*n*-3)	476.00	239.04	43
d_5-C20:5(*n*-3)	474.00	239.04	43
d_5-C22:5(*n*-3)	502.00	239.04	43
d_5-C24:5(*n*-3)	530.00	239.04	43
d_5-C24:6(*n*-3)	528.00	239.04	43
d_5-C26:6(*n*-3)	556.00	239.04	43

[a] Precursor ion is $[M + H]^+$.

Construction of HACD KO cells

To obtain *HACD1* KO, *HACD2* KO, *HACD3* KO, and *HACD1 HACD2* DKO cells, HAP1 cells were transfected with the pYU417 vector (for the control), the pYU-HACD1-CC1-2 and pYU-HACD1-CC1-3 plasmids (for *HACD1* KO), the pYU-HACD2-CC1-1 and pYU-HACD2-CC1-2 plasmids (for *HACD2* KO), the pYU-HACD3-CC2-1 and pYU-HACD3-CC2-2 plasmids (for *HACD3* KO), or the pX330A-puro-HACD1/2 plasmid (for *HACD1 HACD2* DKO). Twenty-four hours after transfection, cells were treated with 2 μg/ml puromycin for 2 days. They were then cultured in Iscove's modified Dulbecco's medium without puromycin for an additional 6 days. Several colonies were selected, and clones with mutations in the genes of interest were used for further study. The mutations in the selected KO/DKO cells were as follows: *HACD1* KO cells, 84-bp deletion (26-bp deletion in exon 1 and 58-bp deletion in intron 1); *HACD2* KO cells, 33-bp deletion plus 77-bp insertion in exon 1; *HACD3* KO cells, 26-bp deletion in exon 4; and *HACD1 HACD2* DKO cells, 33-bp deletion (23-bp deletion in exon 1 and 10-bp deletion in intron 1) in *HACD1* gene and 145-bp deletion (53-bp deletion in exon 1 and 92-bp deletion in intron 1) in *HACD2* gene.

Author contributions—M. S. and Y. U. designed and performed the experiments. M. S., Y. U., Y. O., and M. M. analyzed the data. Y. O., C. N., S. I., and T. S. prepared the *Hacd1* KO mice. A. K. planned and organized the project and wrote the manuscript.

Acknowledgments—We thank Kohei Monobe and Saki Kuwahara for technical assistance.

References

1. Revardel, E., Bonneau, M., Durrens, P., and Aigle, M. (1995) Characterization of a new gene family developing pleiotropic phenotypes upon mutation in *Saccharomyces cerevisiae*. *Biochim. Biophys. Acta* **1263,** 261–265
2. Kohlwein, S. D., Eder, S., Oh, C. S., Martin, C. E., Gable, K., Bacikova, D., and Dunn, T. (2001) Tsc13p is required for fatty acid elongation and localizes to a novel structure at the nuclear-vacuolar interface in *Saccharomyces cerevisiae*. *Mol. Cell. Biol.* **21,** 109–125
3. Han, G., Gable, K., Kohlwein, S. D., Beaudoin, F., Napier, J. A., and Dunn, T. M. (2002) The *Saccharomyces cerevisiae YBR159w* gene encodes the 3-ketoreductase of the microsomal fatty acid elongase. *J. Biol. Chem.* **277,** 35440–35449
4. Denic, V., and Weissman, J. S. (2007) A molecular caliper mechanism for determining very long-chain fatty acid length. *Cell* **130,** 663–677
5. Rantakari, P., Lagerbohm, H., Kaimainen, M., Suomela, J. P., Strauss, L., Sainio, K., Pakarinen, P., and Poutanen, M. (2010) Hydroxysteroid (17β) dehydrogenase 12 is essential for mouse organogenesis and embryonic survival. *Endocrinology* **151,** 1893–1901
6. Kihara, A. (2012) Very long-chain fatty acids: elongation, physiology and related disorders. *J. Biochem.* **152,** 387–395
7. Kihara, A. (2016) Synthesis and degradation pathways, functions, and pathology of ceramides and epidermal acylceramides. *Prog. Lipid Res.* **63,** 50–69
8. Schneiter, R., Hitomi, M., Ivessa, A. S., Fasch, E. V., Kohlwein, S. D., and Tartakoff, A. M. (1996) A yeast acetyl coenzyme A carboxylase mutant links very-long-chain fatty acid synthesis to the structure and function of the nuclear membrane-pore complex. *Mol. Cell. Biol.* **16,** 7161–7172
9. David, D., Sundararabu, S., and Gerst, J. E. (1998) Involvement of long chain fatty acid elongation in the trafficking of secretory vesicles in yeast. *J. Cell Biol.* **143,** 1167–1182
10. Iwabuchi, K., Prinetti, A., Sonnino, S., Mauri, L., Kobayashi, T., Ishii, K., Kaga, N., Murayama, K., Kurihara, H., Nakayama, H., Yoshizaki, F., Takamori, K., Ogawa, H., and Nagaoka, I. (2008) Involvement of very long fatty acid-containing lactosylceramide in lactosylceramide-mediated superoxide generation and migration in neutrophils. *Glycoconj. J.* **25,** 357–374
11. Ohno, Y., Suto, S., Yamanaka, M., Mizutani, Y., Mitsutake, S., Igarashi, Y., Sassa, T., and Kihara, A. (2010) ELOVL1 production of C24 acyl-CoAs is linked to C24 sphingolipid synthesis. *Proc. Natl. Acad. Sci. U.S.A.* **107,** 18439–18444
12. Obara, K., Kojima, R., and Kihara, A. (2013) Effects on vesicular transport pathways at the late endosome in cells with limited very long-chain fatty acids. *J. Lipid Res.* **54,** 831–842
13. Sassa, T., Ohno, Y., Suzuki, S., Nomura, T., Nishioka, C., Kashiwagi, T., Hirayama, T., Akiyama, M., Taguchi, R., Shimizu, H., Itohara, S., and Kihara, A. (2013) Impaired epidermal permeability barrier in mice lacking the *Elovl1* gene responsible for very long-chain fatty acid production. *Mol. Cell. Biol.* **33,** 2787–2796
14. Imgrund, S., Hartmann, D., Farwanah, H., Eckhardt, M., Sandhoff, R., Degen, J., Gieselmann, V., Sandhoff, K., and Willecke, K. (2009) Adult ceramide synthase 2 (CERS2)-deficient mice exhibit myelin sheath defects, cerebellar degeneration, and hepatocarcinomas. *J. Biol. Chem.* **284,** 33549–33560
15. Pewzner-Jung, Y., Brenner, O., Braun, S., Laviad, E. L., Ben-Dor, S., Feldmesser, E., Horn-Saban, S., Amann-Zalcenstein, D., Raanan, C., Berkutzki, T., Erez-Roman, R., Ben-David, O., Levy, M., Holzman, D., Park, H., *et al.* (2010) A critical role for ceramide synthase 2 in liver homeostasis: II. insights into molecular changes leading to hepatopathy. *J. Biol. Chem.* **285,** 10911–10923
16. Aldahmesh, M. A., Mohamed, J. Y., Alkuraya, H. S., Verma, I. C., Puri, R. D., Alaiya, A. A., Rizzo, W. B., and Alkuraya, F. S. (2011) Recessive mutations in *ELOVL4* cause ichthyosis, intellectual disability, and spastic quadriplegia. *Am. J. Hum. Genet.* **89,** 745–750
17. Ben-David, O., Pewzner-Jung, Y., Brenner, O., Laviad, E. L., Kogot-Levin, A., Weissberg, I., Biton, I. E., Pienik, R., Wang, E., Kelly, S., Alroy, J., Raas-Rothschild, A., Friedman, A., Brügger, B., Merrill, A. H., Jr, and Futerman, A. H. (2011) Encephalopathy caused by ablation of very long acyl chain ceramide synthesis may be largely due to reduced galactosylceramide levels. *J. Biol. Chem.* **286,** 30022–30033
18. Harkewicz, R., Du, H., Tong, Z., Alkuraya, H., Bedell, M., Sun, W., Wang, X., Hsu, Y. H., Esteve-Rudd, J., Hughes, G., Su, Z., Zhang, M., Lopes, V. S., Molday, R. S., Williams, D. S., Dennis, E. A., and Zhang, K. (2012) Essential role of ELOVL4 protein in very long chain fatty acid synthesis and retinal function. *J. Biol. Chem.* **287,** 11469–11480
19. Rabionet, M., Bayerle, A., Jennemann, R., Heid, H., Fuchser, J., Marsching, C., Porubsky, S., Bolenz, C., Guillou, F., Gröne, H. J., Gorgas, K., and Sandhoff, R. (2015) Male meiotic cytokinesis requires ceramide synthase 3-dependent sphingolipids with unique membrane anchors. *Hum. Mol. Genet.* **24,** 4792–4808
20. Ohno, Y., Nakamichi, S., Ohkuni, A., Kamiyama, N., Naoe, A., Tsujimura, H., Yokose, U., Sugiura, K., Ishikawa, J., Akiyama, M., and Kihara, A. (2015) Essential role of the cytochrome P450 CYP4F22 in the production of acylceramide, the key lipid for skin permeability barrier formation. *Proc. Natl. Acad. Sci. U.S.A.* **112,** 7707–7712
21. Ohno, Y., Kamiyama, N., Nakamichi, S., and Kihara, A. (2017) PNPLA1 is a transacylase essential for the generation of the skin barrier lipid ω-*O*-acylceramide. *Nat. Commun.* **8,** 14610
22. Sassa, T., and Kihara, A. (2014) Metabolism of very long-chain fatty acids: genes and pathophysiology. *Biomol. Ther.* **22,** 83–92
23. Nugteren, D. H. (1965) The enzymic chain elongation of fatty acids by rat-liver microsomes. *Biochim. Biophys. Acta* **106,** 280–290
24. Oh, C. S., Toke, D. A., Mandala, S., and Martin, C. E. (1997) *ELO2* and *ELO3*, homologues of the *Saccharomyces cerevisiae ELO1* gene, function in fatty acid elongation and are required for sphingolipid formation. *J. Biol. Chem.* **272,** 17376–17384
25. Moon, Y. A., and Horton, J. D. (2003) Identification of two mammalian reductases involved in the two-carbon fatty acyl elongation cascade. *J. Biol. Chem.* **278,** 7335–7343
26. Ikeda, M., Kanao, Y., Yamanaka, M., Sakuraba, H., Mizutani, Y., Igarashi, Y., and Kihara, A. (2008) Characterization of four mammalian 3-hydroxyacyl-CoA dehydratases involved in very long-chain fatty acid synthesis. *FEBS Lett.* **582,** 2435–2440
27. Wang, B., Pelletier, J., Massaad, M. J., Herscovics, A., and Shore, G. C. (2004) The yeast split-ubiquitin membrane protein two-hybrid screen identifies BAP31 as a regulator of the turnover of endoplasmic reticulum-associated protein tyrosine phosphatase-like B. *Mol. Cell. Biol.* **24,** 2767–2778
28. Li, D., Gonzalez, O., Bachinski, L. L., and Roberts, R. (2000) Human protein tyrosine phosphatase-like gene: expression profile, genomic structure, and mutation analysis in families with ARVD. *Gene* **256,** 237–243
29. Pelé, M., Tiret, L., Kessler, J. L., Blot, S., and Panthier, J. J. (2005) SINE exonic insertion in the *PTPLA* gene leads to multiple splicing defects and segregates with the autosomal recessive centronuclear myopathy in dogs. *Hum. Mol. Genet.* **14,** 1417–1427
30. Muhammad, E., Reish, O., Ohno, Y., Scheetz, T., Deluca, A., Searby, C., Regev, M., Benyamini, L., Fellig, Y., Kihara, A., Sheffield, V. C., and Parvari, R. (2013) Congenital myopathy is caused by mutation of *HACD1*. *Hum. Mol. Genet.* **22,** 5229–5236
31. Blondelle, J., Ohno, Y., Gache, V., Guyot, S., Storck, S., Blanchard-Gutton, N., Barthélémy, I., Walmsley, G., Rahier, A., Gadin, S., Maurer, M., Guillaud, L., Prola, A., Ferry, A., Aubin-Houzelstein, G., *et al.* (2015) HACD1, a regulator of membrane composition and fluidity, promotes myoblast fusion and skeletal muscle growth. *J. Mol. Cell. Biol.* **7,** 429–440
32. Kihara, A., Sakuraba, H., Ikeda, M., Denpoh, A., and Igarashi, Y. (2008) Membrane topology and essential amino acid residues of Phs1, a 3-hydroxyacyl-CoA dehydratase involved in very long-chain fatty acid elongation. *J. Biol. Chem.* **283,** 11199–11209
33. Yazawa, T., Naganuma, T., Yamagata, M., and Kihara, A. (2013) Identification of residues important for the catalysis, structure maintenance, and substrate specificity of yeast 3-hydroxyacyl-CoA dehydratase Phs1. *FEBS Lett.* **587,** 804–809
34. Ejsing, C. S., Sampaio, J. L., Surendranath, V., Duchoslav, E., Ekroos, K., Klemm, R. W., Simons, K., and Shevchenko, A. (2009) Global analysis of the yeast lipidome by quantitative shotgun mass spectrometry. *Proc. Natl. Acad. Sci. U.S.A.* **106,** 2136–2141

35. Kastaniotis, A. J., Autio, K. J., Sormunen, R. T., and Hiltunen, J. K. (2004) Htd2p/Yhr067p is a yeast 3-hydroxyacyl-ACP dehydratase essential for mitochondrial function and morphology. *Mol. Microbiol.* **53,** 1407–1421
36. Wakashima, T., Abe, K., and Kihara, A. (2014) Dual functions of the *trans*-2-enoyl-CoA reductase TER in the sphingosine 1-phosphate metabolic pathway and in fatty acid elongation. *J. Biol. Chem.* **289,** 24736–24748
37. Naganuma, T., Sato, Y., Sassa, T., Ohno, Y., and Kihara, A. (2011) Biochemical characterization of the very long-chain fatty acid elongase ELOVL7. *FEBS Lett.* **585,** 3337–3341
38. Abe, K., Ohno, Y., Sassa, T., Taguchi, R., Çalışkan, M., Ober, C., and Kihara, A. (2013) Mutation for nonsyndromic mental retardation in the *trans*-2-enoyl-CoA reductase *TER* gene involved in fatty acid elongation impairs the enzyme activity and stability, leading to change in sphingolipid profile. *J. Biol. Chem.* **288,** 36741–36749
39. Naganuma, T., and Kihara, A. (2014) Two modes of regulation of the fatty acid elongase ELOVL6 by the 3-ketoacyl-CoA reductase KAR in the fatty acid elongation cycle. *PLoS ONE* 9:e101823
40. Steimle, A., Autenrieth, I. B., and Frick, J. S. (2016) Structure and function: lipid A modifications in commensals and pathogens. *Int. J. Med. Microbiol.* **306,** 290–301
41. Lee, E. C., Yu, D., Martinez de Velasco, J., Tessarollo, L., Swing, D. A., Court, D. L., Jenkins, N. A., and Copeland, N. G. (2001) A highly efficient *Escherichia coli*-based chromosome engineering system adapted for recombinogenic targeting and subcloning of BAC DNA. *Genomics* **73,** 56–65
42. Adams, D. J., Quail, M. A., Cox, T., van der Weyden, L., Gorick, B. D., Su, Q., Chan, W. I., Davies, R., Bonfield, J. K., Law, F., Humphray, S., Plumb, B., Liu, P., Rogers, J., and Bradley, A. (2005) A genome-wide, end-sequenced 129Sv BAC library resource for targeting vector construction. *Genomics* **86,** 753–758
43. Kihara, A., Anada, Y., and Igarashi, Y. (2006) Mouse sphingosine kinase isoforms SPHK1a and SPHK1b differ in enzymatic traits including stability, localization, modification, and oligomerization. *J. Biol. Chem.* **281,** 4532–4539
44. Sakuma, T., Nishikawa, A., Kume, S., Chayama, K., and Yamamoto, T. (2014) Multiplex genome engineering in human cells using all-in-one CRISPR/Cas9 vector system. *Sci. Rep.* **4,** 5400
45. Kitamura, T., Seki, N., and Kihara, A. (2017) Phytosphingosine degradation pathway includes fatty acid α-oxidation reactions in the endoplasmic reticulum. *Proc. Natl. Acad. Sci. U.S.A.* **114,** E2616–E2623
46. Brachmann, C. B., Davies, A., Cost, G. J., Caputo, E., Li, J., Hieter, P., and Boeke, J. D. (1998) Designer deletion strains derived from *Saccharomyces cerevisiae* S288C: a useful set of strains and plasmids for PCR-mediated gene disruption and other applications. *Yeast* **14,** 115–132
47. Winzeler, E. A., Shoemaker, D. D., Astromoff, A., Liang, H., Anderson, K., Andre, B., Bangham, R., Benito, R., Boeke, J. D., Bussey, H., Chu, A. M., Connelly, C., Davis, K., Dietrich, F., Dow, S. W., *et al.* (1999) Functional characterization of the *S. cerevisiae* genome by gene deletion and parallel analysis. *Science* **285,** 901–906
48. Kitamura, T., Takagi, S., Naganuma, T., and Kihara, A. (2015) Mouse aldehyde dehydrogenase ALDH3B2 is localized to lipid droplets via two C-terminal tryptophan residues and lipid modification. *Biochem. J.* **465,** 79–87
49. Kondo, N., Ohno, Y., Yamagata, M., Obara, T., Seki, N., Kitamura, T., Naganuma, T., and Kihara, A. (2014) Identification of the phytosphingosine metabolic pathway leading to odd-numbered fatty acids. *Nat. Commun.* **5,** 5338
50. Carette, J. E., Raaben, M., Wong, A. C., Herbert, A. S., Obernosterer, G., Mulherkar, N., Kuehne, A. I., Kranzusch, P. J., Griffin, A. M., Ruthel, G., Dal Cin, P., Dye, J. M., Whelan, S. P., Chandran, K., and Brummelkamp, T. R. (2011) Ebola virus entry requires the cholesterol transporter Niemann-Pick C1. *Nature* **477,** 340–343
51. Liu, L., Cheung, T. H., Charville, G. W., and Rando, T. A. (2015) Isolation of skeletal muscle stem cells by fluorescence-activated cell sorting. *Nat. Protoc.* **10,** 1612–1624

The 3-hydroxyacyl-CoA dehydratases HACD1 and HACD2 exhibit functional redundancy and are active in a wide range of fatty acid elongation pathways

Megumi Sawai, Yukiko Uchida, Yusuke Ohno, Masatoshi Miyamoto, Chieko Nishioka, Shigeyoshi Itohara, Takayuki Sassa and Akio Kihara

J. Biol. Chem. 2017, 292:15538-15551.
doi: 10.1074/jbc.M117.803171 originally published online August 7, 2017